Channel Path Loss Prediction Using Satellite Images: A Deep Learning Approach

Chenlong Wang, *Student Member, IEEE*, Bo Ai, *Fellow, IEEE*, Ruisi He, *Member, IEEE*, Mi Yang, *Member, IEEE*, Shun Zhou, Long Yu, Yuxin Zhang, *Student Member, IEEE*, Zhicheng Qiu, Zhangdui Zhong, *Fellow, IEEE*, Jianhua Fan

***Abstract*—With the advancement of communication technology, there is a higher demand for high-precision and high-generalization channel path loss models as it is fundamental to communication systems. For traditional stochastic and deterministic models, it is difficult to strike a balance between prediction accuracy and generalizability. This paper proposes a novel deep learning-based path loss prediction model using satellite images. In order to efficiently extract environment features from satellite images, residual structure, attention mechanism, and spatial pyramid pooling layer are developed in the network based on expert knowledge. Using a convolutional network activation visualization method, the interpretability of the proposed model is improved. Finally, the proposed model achieves a prediction accuracy with a root mean square error of 5.05 dB, demonstrating an improvement of 3.07 dB over a reference empirical propagation model.**

***Index Terms*—Deep learning, satellite images, channel prediction, path loss.**

I. Introduction

With the continuous development of communication technology, there has been significant improvement in performance, capacity, and user experience of communication systems. Wireless channel plays a crucial role as it determines system performance [1]. With the increasing number of dimensions and enhanced resolution at higher frequencies, channel model accuracy and generalization capability requirements have become increasingly demanding [2].

The environment is of significant importance for propagation, contributing to the complexity of the wireless channel [3]. Channel models depict the impact of interacting objects (IOs) within the environment on propagation. Hence, effective utilization of environment features improves the accuracy of channel models. Traditionally, there are two main types of channel models: statistical models and deterministic models. Statistical models quantify channel characteristics that significantly influence system performance within a specific scenario, utilizing measurement data to fit parameters [4]. However, statistical models can only provide an average depiction of channel parameters. Most statistical models require handcrafted features, such as correction factors in Hata and LEE models [1]. When the terrain changes, a significant amount of parameter adjustments is needed, limiting model accuracy and generalization capability. Deterministic models, such as ray tracing, calculate signal propagation based on Maxwell equations and environment data. This approach yields high accuracy, but at the cost of higher computational complexity compared to statistical models. Additionally, deterministic models have relatively poor generalization ability, and the model is supposed to be reconfigured and recalculated when IOs in the environment change.

Deep learning (DL), with multiple layers of feature transformation and nonlinear activation functions, has excellent nonlinear fitting ability and flexibility [5] that make it suitable for learning nonlinear channel features. Moreover, compared to statistical and deterministic models, DL-based models can adapt to more complex and diverse environments by automatically extracting general environment features from input data [6]. Consequently, DL-based methods achieve a balance between accuracy and generalizability.

A. Related Work

DL has already been used for channel modeling [7]–[13]. Based on environment databases, handcrafted features are used as model inputs, such as the percentage of buildings between the transmitter (Tx) and receiver (Rx), antenna height, etc., and multilayer perceptron (MLP) networks are constructed to predict received signal strength [14]–[16]. A neural based hybrid system that employs a propagation loss algorithm to assist the MLP network. In [17]–[20], it was found that the radial basis function models can fit measurement data faster and obtain more accurate prediction than MLP by selecting appropriate radial basis functions. Deeper DL models are able to search in a larger hypothesis space, thereby describing channel nonlinear features more accurately [20]. However, handcrafted features are mostly based on statistics and cannot fully represent the environment information that affects propagation, especially

This paper is supported in part by the Fundamental Research Funds for the Central Universities 2024QYBS008; in part by the National Natural Science Foundation of China under Grant 62221001, 62341127, 62431003, 62301022 and U21A20445; in part by the Natural Science Foundation of Jiangsu Province Major Project under Grant BK20212002; in part by the State Key Laboratory of Advanced Rail Autonomous Operation under Grant RCS2022ZZ004 and in part by the Young Elite Scientists Sponsorship Program by CAST under Grant 2022QNRC001. (Corresponding authors: Bo Ai and Ruisi He.)

C. Wang, B. Ai, R. He, M. Yang, Y. Zhang, Z. Qiu and Z. Zhong are with the School of Electronics and Information Engineering and the Frontiers Science Center for Smart High-speed Railway System, Beijing Jiaotong University, Beijing 100044, China (email: wang-chenlong@bjtu.edu.cn, aibo@ieee.org, ruisi.he@bjtu.edu.cn, myang@bjtu.edu.cn, 24115024@bjtu.edu.cn, 22110041@bjtu.edu.cn and zhdzhong@bjtu.edu.cn).

S. Zhou, L. Yu and J. Fan are with the Sixty-third Research Institute, National University of Defense Technology, Nanjing 210007, China (email: zhoushun17, yulong17, fanjianhua17@nudt.edu.cn).

high-dimensional spatial information in real environment. This will affect the prediction accuracy of the model.

To capture environment information more comprehensively, many studies have adopted images as input, such as satellite images, elevation maps, building maps, etc. Currently, models that use images as input focus primarily on large-scale channel parameters, and this paper specifically focuses on path loss prediction. Propagation modeling using images can be classified into three main approaches based on the granularity of input and output. The first approach involves a large-area satellite image or feature map as model input, covering a geographic range of up to 2 km, and returns channel characteristics corresponding to the entire image, such as the path loss exponent and shadow fading [21]–[24]. The second approach still uses a large-area satellite image or feature map as input, but focuses on a narrower geographic range surrounding the Tx, typically between 250 m and 2000 m, and returns channel characteristics for each pixel point in the image [25]–[27]. The third approach, in contrast, uses a small-area satellite image or feature map as input, generally focusing on an area within 250 meters of the Rx, and returns channel characteristics at a specified Rx location [28]–[30]. Usually, computational efficiency and accuracy are mutually constrained. This article focuses on the third type, which is high-precision point-to-point path loss prediction. In [28], the authors propose a multi-input network to predict point-to-point path loss in a campus environment. The input features include satellite images of the area near Rx and measurement parameters between Tx and Rx. [29] further improves the above approach by using a model-aided method. In the campus scenario, the output of the neural network is used as a calibration value for the empirical path loss model, and it is found that the accuracy can be further enhanced. Subsequently, [30] addresses the issue that the amount of channel measurement data is often insufficient for training neural networks based on [29]. Specifically, a transfer learning approach is developed to pre-train the model using extensive simulation data generated by a conventional model, and then the model is fine-tuned to obtain accurate results on the basis of measurement data. However,above models are constrained by the range of input images, which requires all input images to be of the same size. In this case, it is hard for the network to capture the complete environment information of the entire propagation link, since the range of environment features changes with variations in Tx-Rx distance, leading to poor generalization when transitioning to new environments.

Several solutions have emerged to address the above problems. In [31], a network based on self-supervised learning is designed that can calculate the path loss between a specified Tx and Rx in a satellite image. Specifically, a larger satellite image is used as a base map and a mask is applied to extract the effective portion of the Tx-to-Rx link from the satellite image. However, the effective mask only occupies a small portion of the satellite image, leading to a waste of computational resources. In addition, a small zoom factor of the satellite image may not provide sufficient detailed information about the propagation environment, which could affect the accuracy of predictions. In [32], a convolutional neural network (CNN) is designed to predict path loss between specific Tx and Rx locations. The model takes a binary building image from Tx to Rx as input and merges it with a free space path loss (FSPL) map centered on the Tx location in the channel dimension. Due to the fact that the image size is restricted to be a square, Tx and Rx are placed at the two diagonal vertices or at the midpoint of two opposite sides. As the relative position between Tx and Rx changes, the image needs to be scaled to maintain a square aspect ratio. This operation can affect the shape of buildings and roads, potentially leading to inaccurate output. Therefore, improving accuracy and generalization requires further exploration.

B. Contributions

In this paper, we propose a path loss prediction model based on DL using satellite images. The complexity of the proposed model inputs is balanced, aiming to improve accuracy while maintaining generalization capability. Our contributions can be summarized as follows.

1) To improve generalizability and prediction accuracy, an input image feature containing Tx-Rx connectivity and surrounding environment information is designed. Specifically, the image size is variable because of the different distances between Tx and Rx.
2) A model capable of handling variable-size inputs is developed based on channel propagation knowledge. The model is designed based on convolutional layers, and residual structures are employed to improve the model receptive field. In order to enhance the ability to extract spatial features, an attention mechanism is incorporated for both spatial and channel dimensions. In addition, a spatial pyramid pooling layer is designed to preserve spatial features when converting features to a fixed size.
3) A visualization method for the intermediate layer outputs of the model is proposed to validate the effectiveness of the designed satellite image data and the model, demonstrating the reliability of the model generalization ability in new scenarios.

C. Article Organization

Section II introduces the path loss prediction model. Section III describes the measurement data and satellite image data, as well as data pre-processing and feature design. The design, visualization and training process of the proposed model are presented in Section IV. Performance validation is analyzed in Section V. Section VI discusses the issues related to the generalizability and visualization accuracy of the proposed model. Finally, Section VII concludes the paper.

II. Path Loss Prediction model

The classic close-in free space reference distance (CI) path loss model [33] has been widely used to estimate path loss in various environments [34]. It can be expressed as

$$\mathrm{PL}^{\mathrm{CI}}(f_c, d_{3\mathrm{D}}) \;=\; \mathrm{FSPL}(f_c, d_0) \;+\; 10n\log_{10}(d_{3D}), \quad (1)$$

where n is the path loss exponent, which can be obtained by minimizing the mean square error (MSE). d_{3D} is the Euclidean distance between Tx and Rx, and it should be larger than 1m [35]. $\text{FSPL}(f_c, d_0)$ is the free space path loss with frequency f_c at a physically-based reference distance d_0 which is 1m in this paper. The CI model can be used as reference for comparison in this paper.

For DL-based path loss prediction models with feature images, the input data generally consists of two types: feature images containing propagation environment information and system parameter vectors based on expert knowledge, such as Tx height, Tx power and Tx-Rx distance. The architecture of the model can typically be divided into three parts. The first part involves using CNN to extract environment features from images, which converts the image input into a one-dimensional environment feature vector. The second part involves employing an MLP to extract features from the system parameter vector and producing a one-dimensional feature vector. Finally, in the third part, the extracted features of the first two parts are combined and fed into an MLP for path loss prediction.

In order to maintain computational efficiency while using fine-grained environment features, it is important to select the necessary range of environment features based on a specific Tx-Rx location. However, existing models are limited by the fixed-size input of satellite images, such as 256×256, which contributes to the inefficient utilization of environment features. The limitation of a fixed input size primarily arises from the fully connected layers used after convolutional layers. These layers have a strict size limit for the input data. The fully connected layer is shown below:

$$h = g(w^T x + c), \tag{2}$$

where w is a linearly varying weight matrix and its size is determined by the input feature x and the output feature h. c is bias term. g is an activation function, also known as a nonlinear function, such as Rectified Linear Unit (ReLU) and sigmoid. The input data dimension of the fully connected layer is fixed when the network is established. A common MLP structure is shown in Fig. 1(a).

The convolutional layer can be described as

$$s(t) = x(a)w(t-a)da, \tag{3}$$

where w is the convolutional kernel and x is the input image. t represents a specific position in the output feature map, and a represents a position in the input image x. There is no size limit for the input of a convolutional layer because it calculates by sliding the convolutional kernel w over image to determine if this pattern exists at different locations. Therefore, with variations in input size, the convolutional layer is still able to recognize the same pattern, even if it is in a different location, as shown in Fig. 1(b).

To address the limitation of input size, an effective approach is to add a global average pooling (GAP) layer or a global maximum pooling (GMP) layer after the CNN before entering it into MLP. However, global pooling can result in loss of location information in the feature map, which is indispensable for the inference of propagation information.

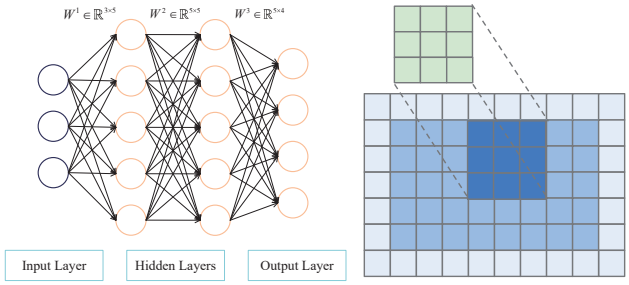

Fig. 1. Classical Model Architecture. (a) Schematic diagram of 3 layers MLP structure, where the hidden layer does not calculate the bias. The sizes of W_1, W_2, and W_3 are fixed when constructing the MLP, so only a fixed input dimension can be inputted. (b) Convolution Calculation Illustration. The green rectangle represents the convolutional kernel, and the light blue color indicates the size of the input image. The dark blue rectangle represents the computation area of the convolutional kernel on the image. The gray area represents the extendable range of the input image. The convolutional kernel slides over the image to perform computations, generating feature maps of different sizes when operating on images of different sizes (gray area).

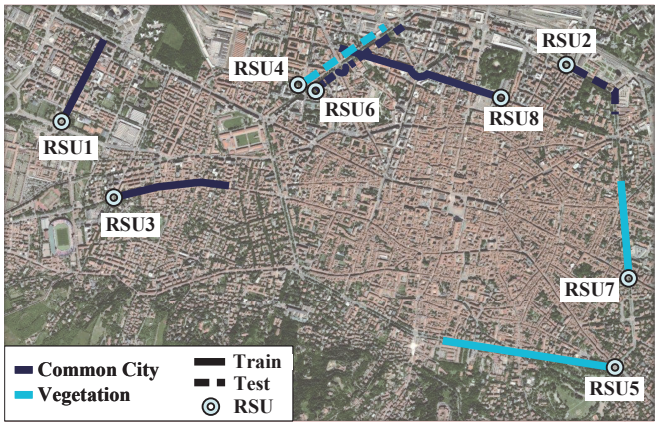

Fig. 2. An overview of data map collected in Bologna, Italy. Solid lines represent the measured data of this route used as training set, while dashed lines represent the measured data of this route used as test set. Different colors represent different environment types. The concentric circles connected to the lines represent Tx locations corresponding to the respective measurement routes.

III. Dataset Construction

In this section, path loss dataset collection and satellite image design are first presented. Data preprocessing and the splitting of dataset are then described in detail.

A. Channel Measurement

We employ an open source dataset [36], where the measurement campaign was performed in a vehicle-to-infrastructure (V2I) scenario in Bologna, and the geographical locations of the measurement data can be observed from Fig. 2. The dataset includes 8 different roadside unit (RSU) locations as Tx locations. The frequency band of the measurement dataset is 5.9 GHz. The Tx heights are set at 6.5 and 10.5 meters, while the Rx is mounted on the roof of a car at approximately 2.5 meters. Given that the measurements were conducted in urban areas, we assume that the Rx height remains constant throughout the measurement campaign. Large-scale channel parameters are provided as received signal strength indicators

(RSSI) in the original dataset. In this article, path loss is calculated through the RSSI [1] and calibrated for antenna pattern and cable loss [36], which can be described in the logarithmic scale as

$$PL = P_{\text{Tx}} - P_{\text{Rx}} + L_{\text{cable}} - G_{\text{Tx}} - G_{\text{Rx}}, \tag{4}$$

where P_{Tx} is the transmission power, and P_{Rx} is the received power, which in this context is the measured RSSI value, L_{cable} represents the cable loss, and G_{Tx} and G_{Rx} are the Tx and Rx antenna gains, respectively.

B. Satellite Images Collection and Processing

As the distance between Tx and Rx varies, the size of the environmental image affecting propagation also changes. As shown in Fig. 3, this variation in size is difficult to quantify using fixed-size features. Therefore, we have defined a new input image. For each satellite image, the Tx and Rx are fixed on the left and right sides, respectively. To ensure sufficient feature information, satellite images are set to a zoom level of 16, where each pixel corresponds to a ground distance of 0.915 meters. This allows for detailed analysis of environment features. The extent of the environmental impact is calculated using the root mean square (RMS) delay spread under Line-of-Sight (LOS) conditions in the UMa scenario, as described in [37]. Specifically, the mean value of the logarithmic RMS delay spread under LOS conditions is calculated as follows:

$$\mu_{\text{LOS}}\ [\text{dB}] = -6.955 - 0.0963 \log_{10}(f_c), \tag{5}$$

where f_c is the frequency in GHz, and the standard deviation σ_{LOS} is 0.66. Considering the lower height of the Tx relative to the UMa scenario and to reduce the amount of input data for the model, we use $\mu_{\text{LOS}} + 0.7\sigma_{\text{LOS}}$ as the extent of the environmental impact, where 0.7 is an empirical value. This corresponds to a distance of approximately 80 meters or 87 pixels. This distance determines the minimum image boundary distance to the Tx and Rx. Satellite image collection in this paper is based on the Mapbox static map API. An example of a satellite image from the dataset is shown in Fig. 4(a). The size of the satellite image is 175 (vertical) $\times$ p (horizontal) $\times$ 3 (RGB color channels), where 175 represents the vertical length of the image, including top and bottom borders (87×2, with an additional 1 pixel for the position of Tx and Rx). p indicates the horizontal length of the image, which varies with the distance of the Tx and Rx.

C. Data Preprocessing

To enable the model to fully comprehend the locations of the Tx and Rx and further learn the propagation mechanism, two feature maps are supplemented: (i) an FSPL map, where pixel values represent the FSPL from the Tx location, and (ii) a distance map, where pixel values represent the distance to the Rx location. These two feature maps are merged with the satellite image along the channel dimension. Ultimately, the combination of these five channels is used as the model input, as illustrated in Fig. 4(b).

Fig. 3. Description of satellite image size. Tx and Rx locations are marked in red and blue. The yellow rectangle represents the size of the intercepted satellite image.

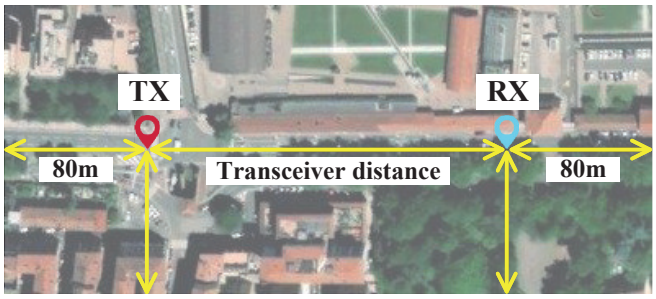

(a)

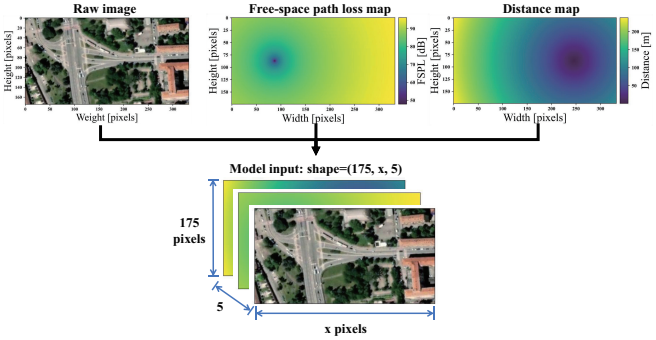

(b)

Fig. 4. Illustration of the model input for the satellite image part. (a) Calculation method of satellite image size. (b) Model input feature map, where the value of x varies with the distance between transceivers.

The original satellite image, with values ranging from 0 to 255, contains three channels. To standardize the satellite image, we normalize each pixel value to the interval [0, 1] by dividing by the maximum value of 255. Since a larger range of images will be used for model prediction, a more stable normalization method for the two feature maps should be employed to enhance the model robustness. In this case, we apply the function $f(x) = \mathrm{e}^{-x}$ to normalize each pixel value in feature maps, ensuring that the Tx-Rx locations on the feature maps are always set to 1. This normalization function maps larger values to a smaller range while preserving the

relative relationships of both FSPL and distance values on feature maps.

The system state information during measurement also contributes to the prediction of path loss. The distance between Tx and Rx, FSPL, and Tx height are used as input features. This feature vector is normalized using $f(x) = \frac{x-\mu}{\sigma}$, where μ is the mean value and σ is the standard deviation of the feature vector.

D. Dataset Splitting

The dataset is categorized based on different environment scenarios: the common city scenario and the tree and vegetation impact scenario. Each measurement activity was conducted independently on a single route. Therefore, in each category, the dataset is divided into training and test sets based on routes as the smallest unit, ensuring that the generalizability of the model can be effectively validated by the test dataset. Dataset splitting is illustrated in Fig. 2. Only RSU 4 and RSU 5 have a height of 10.5 meters, while the heights of the other RSUs are all 6.5 meters. Additionally, 10% of the samples are randomly selected as continuous segments from each measurement route in the training set and combined to form the validation set. The training, validation, and test sets include approximately 16979, 1893, and 13484 samples, respectively. The features of each sample include the satellite image for the specified Tx and Rx location, the Tx and Rx distance, the Tx height, and the FSPL between the Tx and Rx. The label is the path loss value.

IV. Model Design and Implementation

In this section, the architecture and loss function of the proposed model are discussed, and the model implementation is presented.

A. Model Design

We propose a multi-input model capable of extracting features from satellite images and system parameters to predict path loss at a given transceiver location. The model is trained to learn the mapping relationship between the complex environment and path loss values. CNN is applied to extract underlying features from satellite images, while an MLP network is set to handle system state information. Finally, the two sets of features are merged, and an MLP network is developed to predict path loss.

For feature extraction from satellite images, three modules are designed to enable the model to learn effective propagation features and spatial information. Propagation features are complex and abstract, and satellite images contain only visual information of environment features, making it challenging to learn an accurate mapping relationship. We implement a residual link-based architecture [38] for the first module, which allows for the development of deeper models and improves the ability to learn complex functions. Since the transceiver position and relative position of IOs are crucial to propagation, 3×3 and 5×5 size convolutional kernels are used to effectively increase the receptive field of the model. The improved residual blocks are illustrated in Fig. 5.

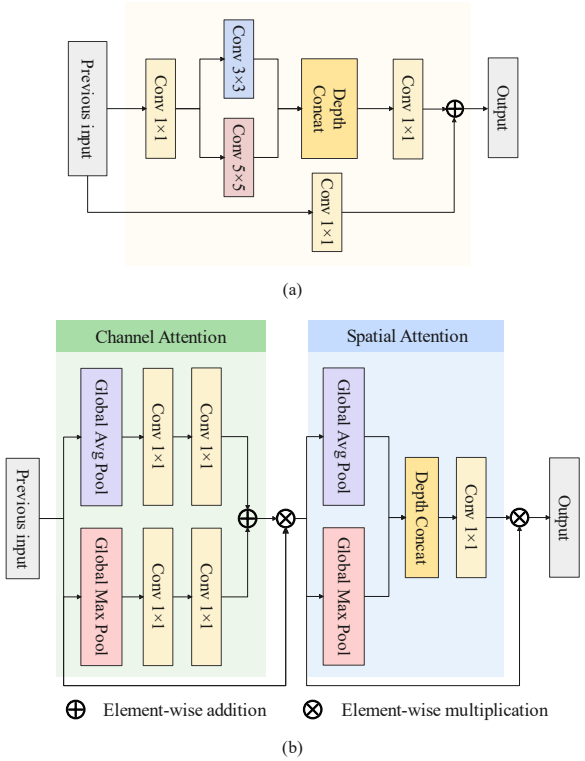

Fig. 5. (a) Modified Resblock architecture with 5×5 convolutional kernel. (b) Attention mechanism architecture.

For the second module, an attention mechanism is employed for both the channel and spatial dimensions inspired by [39]. The attention mechanism in the channel dimension filters the extracted feature patterns, retaining the most effective features. In the spatial dimension, the attention mechanism focuses on the valid parts of feature maps.

To merge the extracted satellite image features with system state information features, it is necessary to convert feature maps of different sizes into the same size. Therefore, we use a spatial pyramid pooling (SPP) layer in the third module to process the output of the convolutional layer, preserving the spatial information of feature maps [40]. SPP divides the feature map into several specified bins and then performs pooling operations on each bin individually, stitching them together to obtain the final result. The pooling operations can be divided into three parts, as illustrated in Fig. 6. The first part directly uses feature map to perform global pooling. In the second and third parts, feature map is horizontally divided into three and five equal parts, respectively. This approach provides different receptive field information for the model, enabling it to focus on the link condition of LOS propagation.

For both the feature extraction of measurement parameters and the final prediction part, we use three-layer MLP networks. The architecture diagram of the model is shown in Fig. 7, and the model parameters can be found in Table I. To avoid overfitting, we apply L_2 kernel regularization with a strength of 10^{-4} on the convolutional layers and dropout with a rate of 0.2 on the fully connected layers. Additionally, all convolutional and fully connected layers use Leaky ReLU as the activation function.

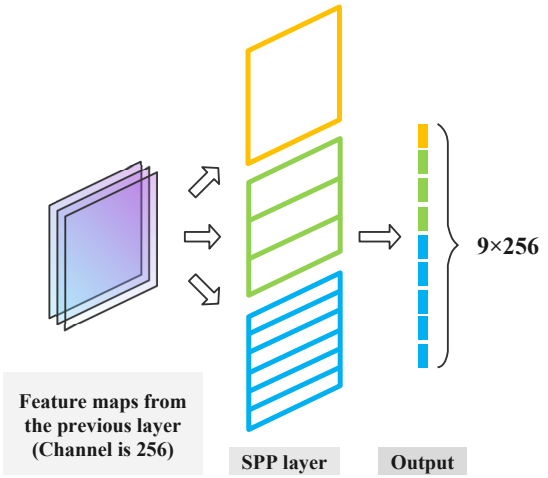

Fig. 6. SPP layer design methodology. The feature map is divided horizontally to highlight the LOS contribution. Feature maps are divided into three different ways. After the division, bins obtained are pooled to obtain vectors with length equals to the number of channels. By concatenating these vectors together, the output result can be obtained.

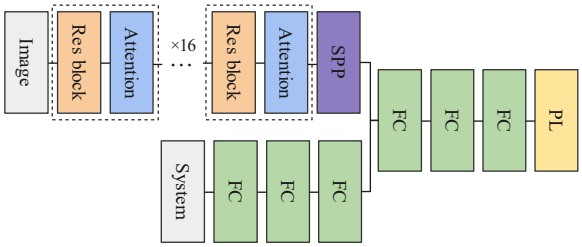

Fig. 7. Improved model architecture. The residual block, attention block, and SPP module are shown in Fig. 5(a), Fig. 5(b), and Fig. 6, respectively.

TABLE I
MODEL ARCHITECTURE DETAILS.

Network	Layer	Output	Description
Satellite Image	Input	(175, p, 5)	/
	Conv Block	(88, p, 32)	7×7, 32, Stride 2
	Res Block 1 $\times 3$	(44, p, 32)	3×3, 32, Stride 2 3×3, 32, Stride 1 5×5, 16, Stride 1 1×1, 32, Stride 1
	Res Block 2 $\times 4$	(22, p, 64)	3×3, 64, Stride 2 3×3, 64, Stride 1 5×5, 32, Stride 1 1×1, 64, Stride 1
	Res Block 3 $\times 6$	(11, p, 128)	...
	Res Block 4 $\times 3$	(6, p, 256)	...
	SPP	(9, 256)	[1, 1], [3, 1], [5, 1]
	Flatten	2304	/
State Information	Input	3	/
	Dense Block 1	10	10
	Dense Block 2	10	10
	Dense Block 3	10	10
Combined Network	Concatenate	2314	/
	Dense Block 1	2048	2048
	Dense Block 2	512	512
	Dense Block 3	1	1

B. Model Interpretability

Model visualization can help understand how model makes predictions [41]–[44]. A common method is to calculate the gradient of the output with respect to a certain activation layer to obtain influence of each part of the activation layer on the final result and then visualize it as an activation map [45]–[47]. In this method, output values are mostly positive, with larger values indicating higher confidence. The ReLU activation function is widely used to remove negative values in activation and gradient maps to enhance visualization performance. However, in the proposed model, output values can be negative, and an increase in the prediction result indicates a stronger signal. Therefore, identifying positive values in the gradient map helps us find the areas in the environment that significant impact signal strength, while the activation map should retain negative values.

To enhance model interpretability, we design a visualization scheme based on [47], which calculates a saliency map to indicate the importance of different locations in the image for model prediction, thus helping us understand how model makes decisions. The saliency map L_{ij}, representing the importance of each spatial position (i, j) for prediction, is calculated as shown in formula 6. Since Leaky ReLU is used as the activation function in the model, leading to negative values in intermediate layers, absolute value calculations are performed to enhance the visualization effect.

$$L_{ij} = \sum_k \left| \text{relu}\left(\frac{\partial Y}{\partial A_{ij}^k} \right) \cdot A_{ij}^k \right|, \tag{6}$$

where A_{ij}^k represents the activation map of the k-th channel in a certain layer. Y represents the prediction result.

C. Model Implementation

In this work, we mainly use TensorFlow 2.10.0 on a workstation equipped with an NVIDIA GeForce RTX 4090 GPU for model training. To avoid the training instability caused by zero-padding when concatenating images of different sizes in a batch, we use the stochastic gradient descent method with a batch size of 1. We employ the random gradient descent method with a batch size of 1. Besides, the Adam optimizer [48] with a learning rate of 0.0001 is used. The two hyperparameters in Adam optimizer, β_1 and β_2, are set to be 0.9 and 0.999, respectively. MSE is employed as the loss function. After training with 300 epochs, the path loss prediction model can be obtained.

V. PERFORMANCE EVALUATION

In this section, we validate the effectiveness and interpretability of the proposed model for environment information

extraction and compare it with previous approaches. Additionally, we compare the gains brought by different model architectures.

A. Environment Information Extraction Effectiveness

Firstly, we compare the path loss prediction accuracy of the proposed model, the CI model, and a prediction model using satellite images near the Rx as input (referred to as the "model with local image"). For the model with local image, we construct a model with the same framework as [28]. The CI model and the model with local image are trained on the same dataset as the proposed model. After fitting, the path loss exponent of the CI model is 2.33. Fig. 8 shows the prediction performance of the above three models on a test dataset under two scenarios: the common city scenario and the tree and vegetation impact scenario. It can be first observed that the CI model only captures the overall trend of path loss and fails to fit well with measurement data due to insufficient utilization of environment information. Furthermore, there is a certain mismatch between the predictions of the model with local image and measurement data. In contrast, the proposed model demonstrates the best prediction accuracy and fitting. Additionally, the RMSE at different distances between the

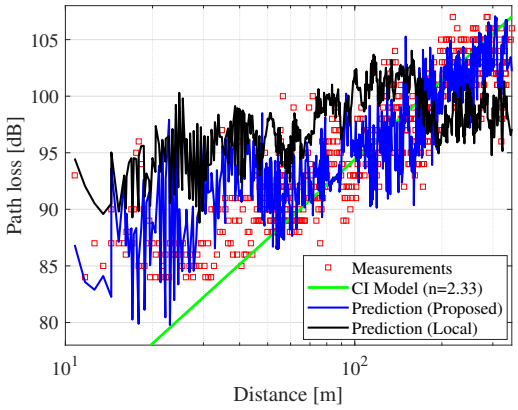

(a)

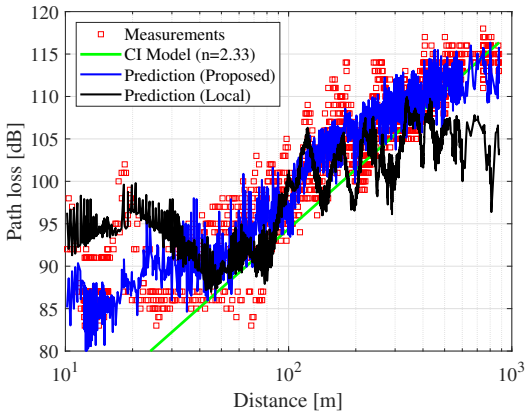

(b)

Fig. 8. Comparison of model prediction accuracy for different scenarios. (a) Testing route for common city scenario. (b) Testing route for trees and vegetation scenario.

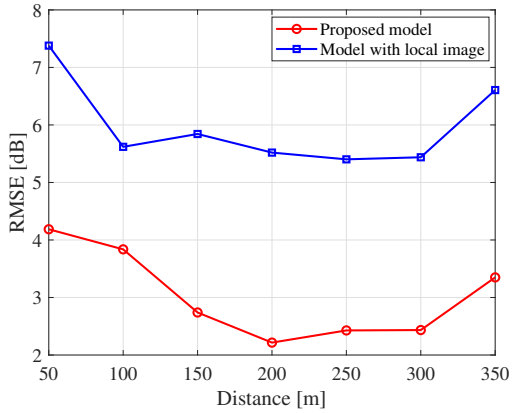

Fig. 9. Average RMSE versus distance in the test route for the common city scenario. Each point represents the average RMSE with a bin size of 50m.

proposed model and the model with local image is compared, as in Fig. 9. Specifically, the route is divided into 50 m bins, and the average RMSE is calculated for all points within each bin. The proposed model outperforms the model with local image at all distances.

The performance of different models is validated using RMSE based on all routes in the test set. The prediction accuracy is depicted using a box plot in Fig. 10. The top and bottom edges of the boxes represent the first and third quartiles, respectively, and the boxes contains 50% of the error results. The whiskers extend to the remaining data, with the top and bottom ends of the whiskers representing the maximum and minimum values, respectively. We also verify the average RMSE, mean absolute percentage error (MAPE) and Pearson correlation coefficient (PCC) of different models for each test scenario, as shown in Table II, Table III and Table IV. The RMSE, MAPE, and PCC are given by:

$$\text{RMSE} = \sqrt{\frac{1}{N}\sum_{i=1}^{N}(y_i - \hat{y}_i)^2}, \tag{7}$$

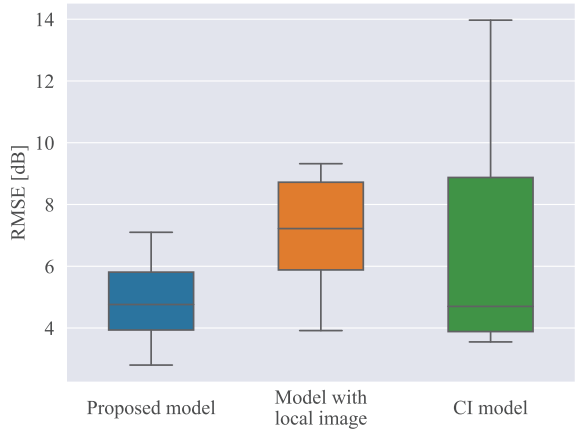

Fig. 10. Boxplot of model prediction accuracy on different test routes. Compute RMSE for models using measurement data from each route in the test dataset.

$$\text{MAPE} = \frac{100}{N}\sum_{i=1}^{N}\left|\frac{y_i - \hat{y}_i}{y_i}\right|, \tag{8}$$

$$\text{PCC} = \frac{\text{cov}(\boldsymbol{y}, \hat{\boldsymbol{y}})}{\sigma_{\boldsymbol{y}}\sigma_{\hat{\boldsymbol{y}}}}, \tag{9}$$

where $\boldsymbol{y} = \{y_1, \ldots, y_N\}$ and $\hat{\boldsymbol{y}} = \{\hat{y}_1, \ldots, \hat{y}_N\}$ refer to the measured and predicted values, respectively. N indicates the number of samples. $\text{cov}(\boldsymbol{y}, \hat{\boldsymbol{y}})$ represents the covariance of $\boldsymbol{y}$ and $\hat{\boldsymbol{y}}$, and $\sigma_{\boldsymbol{y}}$ and $\sigma_{\hat{\boldsymbol{y}}}$ are the standard deviations of $\boldsymbol{y}$ and $\hat{\boldsymbol{y}}$, respectively. In the common city scenario, the propagation environment is relatively simple, with radio waves mainly following a LOS path, exhibiting a log-scale relationship. As a result, the CI model can achieve a better fit, but the proposed model is more prone to overfitting in such a simple environment. According to the Pearson correlation coefficient, the proposed model shows a good correlation with the data in the common city scenario, though it exhibits a certain mean bias during predictions. This issue could be improved in the future through model-aided methods , such as using the output results of the model to compensate for the predictions of a statistical model. In complex scenarios influenced by trees and vegetation, channel characteristics become more nonlinear, and the proposed model outperforms the other two models in terms of prediction accuracy. For the overall test dataset, the proposed model can improve RMSE prediction accuracy by 1.90 dB compared to the model with local image and by 3.07 dB compared to the CI model.

Visualization results of a partial output of the model are presented in Fig. 11, where Tx and Rx locations are marked in red and blue, respectively. In the saliency map, light blue corresponds to important pixels, as opposed to dark blue. In the bottom image, we have marked the most important parts influencing the prediction with yellow dashed lines.

The saliency map clearly highlights the impact of environmental features within the LOS region on the prediction results, confirming the necessity of incorporating environmental information between Tx and Rx in the model input. By observing the important regions within the yellow dashed lines, the model identifies the most crucial areas for pre-

TABLE II
RMSE COMPARISON OF PREDICTION ACCURACY IN DIFFERENT SCENARIOS.

	Proposed model	**Model with local image**	**CI model**
Common City	4.43 dB	6.80 dB	4.02 dB
Trees and Vegetation	5.67 dB	7.13 dB	11.08 dB
All	5.05 dB	6.95 dB	8.12 dB

TABLE III
MAPE COMPARISON OF PREDICTION ACCURACY IN DIFFERENT SCENARIOS.

	Proposed model	**Model with local image**	**CI model**
Common City	4.54 %	6.60 %	2.95 %
Trees and Vegetation	5.58 %	7.77 %	8.49 %
All	5.03 %	7.15 %	5.54 %

TABLE IV
PCC COMPARISON OF PREDICTION ACCURACY IN DIFFERENT SCENARIOS.

	Proposed model	**Model with local image**	**CI model**
Common City	0.90	0.65	0.81
Trees and Vegetation	0.88	0.75	0.90
All	0.85	0.69	0.81

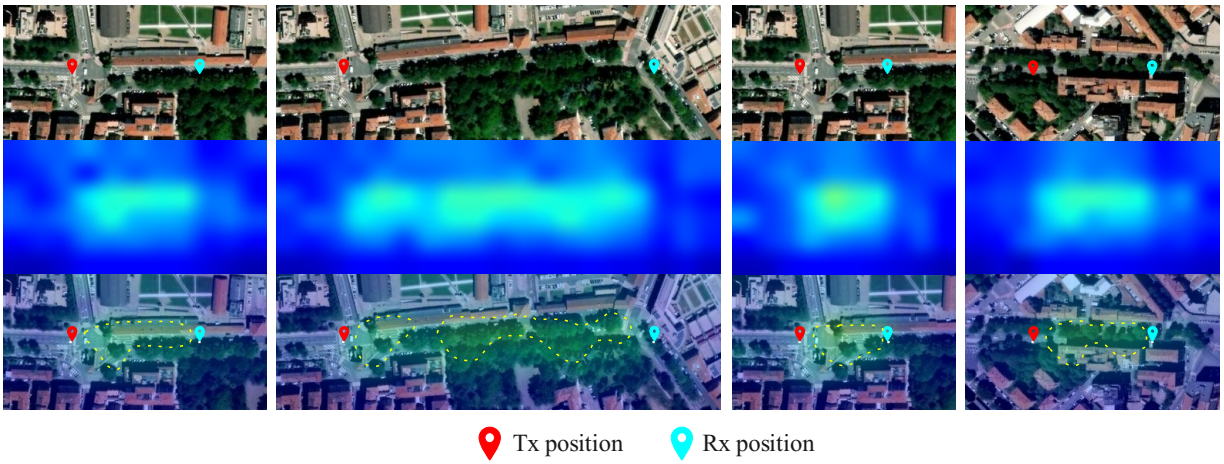

Fig. 11. Visualization results for 4 different input satellite images. The Tx and Rx positions are marked in red and blue, respectively. In saliency map, light blue corresponds to important pixels, as opposed to dark blue. The top image shows the satellite image input to the model, the middle image shows the saliency map calculated based on this input, and the bottom image shows the satellite image with the overlaid saliency map. In the bottom image, we have marked the most important parts influencing the prediction with yellow dashed lines.

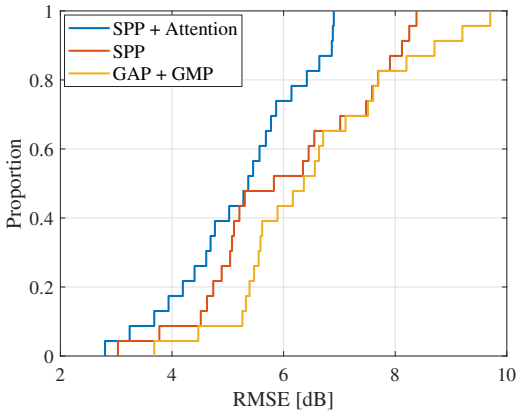

Fig. 12. Model performance improvement comparison.

diction as highly overlapping with the terrain features along the propagation path, such as buildings and vegetation. This illustrates the substantial effect of terrain features on path loss prediction. It can be observed that the importance assigned by the model to the trees and vegetation regions is greater than that to building regions. This may be due to buildings typically causing obstruction and resulting in reflection or refraction, while trees and vegetation areas cause extensive scattering, leading to a larger impact area. Moreover, the model does not extract features only from large areas of vegetation and buildings. Observing the first three visualizations, it can be seen that the model consistently assigns high importance to a single tree located at the bottom right corner of the transmitter. Despite some margin left around the images near the Tx and Rx, it does not significantly affect the prediction results. These findings fully demonstrate that effective feature extraction between Tx and Rx can further enhance the accuracy and effectiveness of the model in path loss prediction.

B. Model architecture validation

We compare the effects of using GAP and GMP, SPP after CNN. Both GAP and GMP are applied to the feature layer output by CNN, and the results obtained by these two methods are concatenated. The experimental results are shown in Fig. 12. Although the SPP method has more parameters, it improves the network prediction accuracy by about 0.52 dB. We also compare the proposed model with and without using the attention mechanism. It can be observed that using the attention mechanism improves the RMSE by about 0.82 dB for the model.

VI. DISCUSSION

A. Model Generalizability

We proposed a path loss prediction model based on satellite images, validating the generalization advantages of using complete satellite image features between the Tx and Rx links as input. While there is still room for improvement in the generalization of the proposed model in other aspects, we will continue to investigate these issues in future work.

1) The colors of satellite images: Since the model extracts environmental features from satellite images, the color information in these images can impact the generalizability of the model. However, in the dataset, most buildings in Bologna have red roofs, causing the model to associate the building information with red roofs. As a result, the generalizability of the model decreases in entirely new scenarios. Similarly, vegetation changes in different seasons can also affect the generalizability. This problem can be addressed by utilizing the subsequent two approaches.

- Environmental Feature Extraction: In the process of designing environmental features, incorporating semantic segmentation results for objects like buildings and vegetation, along with elevation data, can be beneficial. This approach can help minimize color-related interference and aid the model in identifying crucial features that influence propagation, thus enhancing the model's ability to generalize across various environments.
- Expanding the Dataset: Expanding the dataset to include various regions can improve the generalizability of the model. Introducing a diverse range of buildings and natural environments into the training dataset will enable the model to better adapt to new scenarios and avoid relying solely on specific color features for predictions.

2) Frequency Bands and Scenarios: The proposed model supports training and prediction in any frequency band in outdoor scenarios. However, due to the limitations of the dataset, the model's design does not include multi-band feature extraction and prediction, and its generalizability in mixed scenarios still needs to be further validated with corresponding data. In the future, we will explore the generalizability of the model in multi-band complex scenarios.

3) Model Prediction Distance: Due to the dataset constraints, the furthest testable distance is about 1.5 km. Beyond this limit, the model is unable to generate reliable prediction results. This problem can be improved by employing the following two approaches.

- Transfer Learning Method: Use extensive simulated channel data for transfer learning, followed by fine-tuning the model with measured data. This approach leverages the richness of the simulated data while ensuring the model's accuracy in real-world scenarios, thereby improving the issue of unreasonable model predictions at long distances.
- Model-aided Method: Use the output of the DL model as a compensation value for an empirical model or a simple deterministic model. This enhances the stability and accuracy of the model predictions.

B. Model Interpretability Method

The model visualization method is based on the feature maps output by the top convolutional layers. Due to the low resolution of these feature maps, the resulting importance maps also have low resolution. Consequently, the visualization can only highlight key areas in the input image that influence the prediction results, making it difficult to precisely align the important regions with specific scatterers. Future work will explore more refined visualization techniques to explore the

relationship between environmental features and radio wave propagation mechanisms.

VII. CONCLUSION

In this paper, a DL-based path loss prediction model is proposed. The model mainly employs satellite images as input, which contain complete propagation environment information between Tx and Rx. To extract features from images, residual structures, attention mechanisms, and spatial pyramid pooling are designed. In addition, a visualization method is proposed to demonstrate the necessity of considering complete propagation environment information as input. The prediction accuracy of the proposed model is verified by comparing it with the CI model and the prediction model that uses only local satellite images. Results show that the proposed model have better agreement with the measurements, achieving an RMSE of 5.05 dB.

REFERENCES

[1] A. F. Molisch, *Wireless communications*, 2nd ed. Chichester, West Sussex, U.K: Wiley : IEEE, 2011.

[2] M. Yang, B. Ai, R. He, L. Chen, X. Li, J. Li, B. Zhang, C. Huang, and Z. Zhong, "A Cluster-Based Three-Dimensional Channel Model for Vehicle-to-Vehicle Communications," *IEEE Transactions on Vehicular Technology*, vol. 68, no. 6, pp. 5208–5220, Jun. 2019, conference Name: IEEE Transactions on Vehicular Technology.

[3] M. Yang, B. Ai, R. He, Z. Ma, H. Mi, D. Fei, Z. Zhong, Y. Li, and J. Li, "Dynamic V2V Channel Measurement and Modeling at Street Intersection Scenarios," *IEEE Transactions on Antennas and Propagation*, vol. 71, no. 5, pp. 4417–4432, May 2023, conference Name: IEEE Transactions on Antennas and Propagation.

[4] R. He, C. Schneider, B. Ai, G. Wang, Z. Zhong, D. A. Dupleich, R. S. Thomae, M. Boban, J. Luo, and Y. Zhang, "Propagation Channels of 5G Millimeter-Wave Vehicle-to-Vehicle Communications: Recent Advances and Future Challenges," *IEEE Vehicular Technology Magazine*, vol. 15, no. 1, pp. 16–26, Mar. 2020, conference Name: IEEE Vehicular Technology Magazine. [Online]. Available: https://ieeexplore.ieee.org/document/8851421

[5] I. Goodfellow, Y. Bengio, and A. Courville, *Deep Learning*. MIT Press, 2016.

[6] M. Yang, R. He, B. Ai, C. Huang, C. Wang, Y. Zhang, and Z. Zhong, "AI-enabled Data-driven Channel Modeling for Future Communications," *IEEE Communications Magazine*, pp. 1–7, 2023, conference Name: IEEE Communications Magazine.

[7] C. Huang, R. He, B. Ai, A. F. Molisch, B. K. Lau, K. Haneda, B. Liu, C.-X. Wang, M. Yang, C. Oestges, and Z. Zhong, "Artificial Intelligence Enabled Radio Propagation for Communications—Part I: Channel Characterization and Antenna-Channel Optimization," *IEEE Transactions on Antennas and Propagation*, pp. 1–1, 2022.

[8] ——, "Artificial Intelligence Enabled Radio Propagation for Communications—Part II: Scenario Identification and Channel Modeling," *IEEE Transactions on Antennas and Propagation*, pp. 1–1, 2022.

[9] Yang Yang, Yang Li, Wuxiong Zhang, Fei Qin, Pengcheng Zhu, and Cheng-Xiang Wang, "Generative-Adversarial-Network-Based Wireless Channel Modeling: Challenges and Opportunities," *IEEE Communications Magazine*, vol. 57, no. 3, pp. 22–27, Mar. 2019.

[10] Lu Bai, Qian Xu, Ziwei Huang, Shangbin Wu, Spiros Ventouras, George Goussetis, and Xiang Cheng, "An Atmosphere Data Driven Q Band Satellite Channel Model with Feature Selection," *IEEE Transactions on Antennas and Propagation*, pp. 1–1, 2021.

[11] M. Yang, B. Ai, R. He, C. Shen, M. Wen, C. Huang, J. Li, Z. Ma, L. Chen, X. Li, and Z. Zhong, "Machine-Learning-Based Scenario Identification Using Channel Characteristics in Intelligent Vehicular Communications," *IEEE Transactions on Intelligent Transportation Systems*, vol. 22, no. 7, pp. 3961–3974, Jul. 2021, conference Name: IEEE Transactions on Intelligent Transportation Systems. [Online]. Available: https://ieeexplore.ieee.org/document/9123691

[12] R. He, B. Ai, Z. Zhong, M. Yang, R. Chen, J. Ding, Z. Ma, G. Sun, and C. Liu, "5G for Railways: Next Generation Railway Dedicated Communications," *IEEE Communications Magazine*, vol. 60, no. 12, pp. 130–136, Dec. 2022, conference Name: IEEE Communications Magazine. [Online]. Available: https://ieeexplore.ieee.org/abstract/document/9895381

[13] X. Zhao, F. Du, S. Geng, Z. Fu, Z. Wang, Y. Zhang, Z. Zhou, L. Zhang, and L. Yang, "Playback of 5G and Beyond Measured MIMO Channels by an ANN-Based Modeling and Simulation Framework," *IEEE Journal on Selected Areas in Communications*, vol. 38, no. 9, pp. 1945–1954, Sep. 2020.

[14] A. Neskovic, N. Neskovic, and D. Paunovic, "ANN microcell electric field level prediction model," in *EUROCON'2001. International Conference on Trends in Communications. Technical Program, Proceedings (Cat. No.01EX439)*, vol. 1, Jul. 2001, pp. 128–131 vol.1.

[15] E. Ostlin, H.-J. Zepernick, and H. Suzuki, "Macrocell Path-Loss Prediction Using Artificial Neural Networks," *IEEE Transactions on Vehicular Technology*, vol. 59, no. 6, pp. 2735–2747, Jul. 2010.

[16] L. Wu, D. He, K. Guan, B. Ai, C. Briso-Rodríguez, T. Shui, C. Liu, L. Zhu, and X. Shen, "Received Power Prediction for Suburban Environment based on Neural Network," in *2020 International Conference on Information Networking (ICOIN)*, 2020, pp. 35–39.

[17] P.-R. Chang and W.-H. Yang, "Environment-adaptation mobile radio propagation prediction using radial basis function neural networks," *IEEE Transactions on Vehicular Technology*, vol. 46, no. 1, pp. 155–160, 1997.

[18] R. Fraile, L. Rubio, and N. Cardona, "Application of RBF neural networks to the prediction of propagation loss over irregular terrain," in *Vehicular Technology Conference Fall 2000. IEEE VTS Fall VTC2000. 52nd Vehicular Technology Conference (Cat. No.00CH37152)*, vol. 2, Sep. 2000, pp. 878–884 vol.2.

[19] W. Hu, S. Geng, and X. Zhao, "Mm-Wave 60 GHz Channel Fading Effects Analysis Based on RBF Neural Network," in *2020 5th International Conference on Computer and Communication Systems (ICCCS)*, May 2020, pp. 589–593.

[20] A. Seretis and Costas D. Sarris, "An Overview of Machine Learning Techniques for Radiowave Propagation Modeling," *IEEE Transactions on Antennas and Propagation*, pp. 1–1, 2021.

[21] H. F. Ates, S. M. Hashir, T. Baykas, and B. K. Gunturk, "Path Loss Exponent and Shadowing Factor Prediction From Satellite Images Using Deep Learning," *IEEE Access*, vol. 7, pp. 101 366–101 375, 2019.

[22] M. Z. Alam, H. F. Ates, T. Baykas, and B. K. Gunturk, "Analysis of deep learning based path loss prediction from satellite images," in *2021 29th Signal Processing and Communications Applications Conference (SIU)*, Jun. 2021, pp. 1–4.

[23] Omar Ahmadien, Hasan F. Ates, Tuncer Baykas, and Bahadir K. Gunturk, "Predicting Path Loss Distribution of an Area From Satellite Images Using Deep Learning," *IEEE Access*, vol. 8, pp. 64 982–64 991, 2020.

[24] T. Imai, K. Kitao, and M. Inomata, "Radio Propagation Prediction Model Using Convolutional Neural Networks by Deep Learning," in *2019 13th European Conference on Antennas and Propagation (EuCAP)*, Mar. 2019, pp. 1–5.

[25] Vishnu V. Ratnam, Hao Chen, Sameer Pawar, Bingwen Zhang, Charlie Jianzhong Zhang, Young-Jin Kim, Soonyoung Lee, Minsung Cho, and Sung-Rok Yoon, "FadeNet: Deep Learning-Based mm-Wave Large-Scale Channel Fading Prediction and its Applications," *IEEE Access*, vol. 9, pp. 3278–3290, 2021.

[26] Ron Levie, Çağkan Yapar, Gitta Kutyniok, and Giuseppe Caire, "RadioUNet: Fast Radio Map Estimation With Convolutional Neural Networks," *IEEE Transactions on Wireless Communications*, vol. 20, no. 6, pp. 4001–4015, Jun. 2021.

[27] Ahmed Marey, Mustafa Bal, Hasan F. Ates, and Bahadir K. Gunturk, "PL-GAN: Path Loss Prediction using Generative Adversarial Networks," *IEEE Access*, pp. 1–1, 2022.

[28] Jakob Thrane, Matteo Artuso, Darko Zibar, and Henrik L. Christiansen, "Drive Test Minimization Using Deep Learning with Bayesian Approximation," in *2018 IEEE 88th Vehicular Technology Conference (VTC-Fall)*, 2018, pp. 1–5.

[29] Jakob Thrane, Darko Zibar, and Henrik Lehrmann Christiansen, "Model-Aided Deep Learning Method for Path Loss Prediction in Mobile Communication Systems at 2.6 GHz," *IEEE Access*, vol. 8, pp. 7925–7936, 2020.

[30] Thao T. Nguyen, Raied Caromi, Kassem Kallas, and Michael R. Souryal, "Deep Learning for Path Loss Prediction in the 3.5 GHz CBRS Spectrum Band," in *2022 IEEE Wireless Communications and Networking Conference (WCNC)*, Apr. 2022, pp. 1665–1670.

[31] M. Sousa, P. Vieira, M. P. Queluz, and A. Rodrigues, "An Ubiquitous 2.6 GHz Radio Propagation Model for Wireless Networks Using Self-Supervised Learning From Satellite Images," *IEEE Access*, vol. 10, pp. 78 597–78 615, 2022. [Online]. Available: https://ieeexplore.ieee.org/document/9837897

[32] Kazuya Inoue, Koichi Ichige, Tatsuya Nagao, and Takahiro Hayashi, "Learning-Based Prediction Method for Radio Wave Propagation Using Images of Building Maps," *IEEE Antennas and Wireless Propagation Letters*, vol. 21, no. 1, pp. 124–128, 2022.

[33] T. S. Rappaport, Y. Xing, G. R. MacCartney, A. F. Molisch, E. Mellios, and J. Zhang, "Overview of Millimeter Wave Communications for Fifth-Generation (5G) Wireless Networks—With a Focus on Propagation Models," *IEEE Transactions on Antennas and Propagation*, vol. 65, no. 12, pp. 6213–6230, 2017.

[34] G. R. MacCartney and T. S. Rappaport, "Rural Macrocell Path Loss Models for Millimeter Wave Wireless Communications," *IEEE Journal on Selected Areas in Communications*, vol. 35, no. 7, pp. 1663–1677, Jul. 2017.

[35] T. S. Rappaport, G. R. MacCartney, M. K. Samimi, and S. Sun, "Wideband Millimeter-Wave Propagation Measurements and Channel Models for Future Wireless Communication System Design," *IEEE Transactions on Communications*, vol. 63, no. 9, pp. 3029–3056, Sep. 2015.

[36] J. Gozalvez, M. Sepulcre, and R. Bauza, "IEEE 802.11p vehicle to infrastructure communications in urban environments," *IEEE Communications Magazine*, vol. 50, no. 5, pp. 176–183, 2012.

[37] "Study on channel model for frequencies from 0.5 to 100 GHz (3GPP TR 38.901 version 18.0.0 Release 18)."

[38] K. He, X. Zhang, S. Ren, and J. Sun, "Deep Residual Learning for Image Recognition," in *2016 IEEE Conference on Computer Vision and Pattern Recognition (CVPR)*. Las Vegas, NV, USA: IEEE, Jun. 2016, pp. 770–778. [Online]. Available: http://ieeexplore.ieee.org/document/7780459/

[39] S. Woo, J. Park, J.-Y. Lee, and I. S. Kweon, "CBAM: Convolutional Block Attention Module," Jul. 2018. [Online]. Available: http://arxiv.org/abs/1807.06521

[40] K. He, X. Zhang, S. Ren, and J. Sun, "Spatial Pyramid Pooling in Deep Convolutional Networks for Visual Recognition," *IEEE Transactions on Pattern Analysis and Machine Intelligence*, vol. 37, no. 9, pp. 1904–1916, Sep. 2015.

[41] J. T. Springenberg, A. Dosovitskiy, T. Brox, and M. Riedmiller, "Striving for Simplicity: The All Convolutional Net," Apr. 2015. [Online]. Available: http://arxiv.org/abs/1412.6806

[42] M. D. Zeiler and R. Fergus, "Visualizing and Understanding Convolutional Networks," in *Computer Vision – ECCV 2014*, ser. Lecture Notes in Computer Science, D. Fleet, T. Pajdla, B. Schiele, and T. Tuytelaars, Eds. Cham: Springer International Publishing, 2014, pp. 818–833.

[43] B. Zhou, A. Khosla, A. Lapedriza, A. Oliva, and A. Torralba, "Learning Deep Features for Discriminative Localization," 2016, pp. 2921–2929. [Online]. Available: https://openaccess.thecvf.com/content_cvpr_2016/html/Zhou_Learning_Deep_Features_CVPR_2016_paper.html

[44] H. Wang, Z. Wang, M. Du, F. Yang, Z. Zhang, S. Ding, P. Mardziel, and X. Hu, "Score-CAM: Score-Weighted Visual Explanations for Convolutional Neural Networks," 2020, pp. 24–25. [Online]. Available: https://openaccess.thecvf.com/content_CVPRW_2020/html/w1/Wang_Score-CAM_Score-Weighted_Visual_Explanations_for_Convolutional_Neural_Networks_CVPRW_2020_paper.html

[45] R. R. Selvaraju, M. Cogswell, A. Das, R. Vedantam, D. Parikh, and D. Batra, "Grad-CAM: Visual Explanations From Deep Networks via Gradient-Based Localization," 2017, pp. 618–626. [Online]. Available: https://openaccess.thecvf.com/content_iccv_2017/html/Selvaraju_Grad-CAM_Visual_Explanations_ICCV_2017_paper.html

[46] A. Chattopadhay, A. Sarkar, P. Howlader, and V. N. Balasubramanian, "Grad-CAM++: Generalized Gradient-Based Visual Explanations for Deep Convolutional Networks," in *2018 IEEE Winter Conference on Applications of Computer Vision (WACV)*, Mar. 2018, pp. 839–847.

[47] P.-T. Jiang, C.-B. Zhang, Q. Hou, M.-M. Cheng, and Y. Wei, "LayerCAM: Exploring Hierarchical Class Activation Maps for Localization," *IEEE Transactions on Image Processing*, vol. 30, pp. 5875–5888, 2021.

[48] D. P. Kingma and J. Ba, "Adam: A Method for Stochastic Optimization," *arXiv:1412.6980 [cs]*, Jan. 2017. [Online]. Available: http://arxiv.org/abs/1412.6980

CHENLONG WANG received the B.S. degree in communication engineering from Henan University, Henan, China, in 2021. He is currently pursuing the Ph.D. degree with the School of Electronics and Information Engineering, Beijing Jiaotong University, Beijing, China. His current research is the application of machine learning to wireless channel modeling.

BO AI (Fellow, IEEE) received the M.S. and Ph.D. degrees from Xidian University, China.

He studies as a postdoctoral student with Tsinghua University. He was a Visiting Professor with the Electrical Engineering Department, Stanford University in 2015. He is currently with Beijing Jiaotong University as a Full Professor and a Ph.D. Candidate Advisor, where he is the Director of the School of Electronic and Information Engineering. He is one of the main people responsible for the Beijing Urban Rail Operation Control System, International Science and Technology Cooperation Base. He is also a member of the Innovative Engineering Based jointly granted by the Chinese Ministry of Education and the State Administration of Foreign Experts Affairs. He was honored with the Excellent Postdoctoral Research Fellow by Tsinghua University in 2007. He has authored/coauthored eight books and published over 300 academic research papers in his research area. He holds 26 invention patents. He has been the research team leader for 26 national projects. His interests include the research and applications of channel measurement and channel modeling and dedicated mobile communications for rail traffic systems. He has been notified by the Council of Canadian Academies that, based on Scopus database, he has been listed as one of the Top 1% authors in his field all over the world. He has also been feature interviewed by the IET Electronics Letters. He has received some important scientific research prizes.

RUISI HE received the B.E. and Ph.D. degrees from Beijing Jiaotong University (BJTU), Beijing, China, in 2009 and 2015, respectively.

Dr. He is currently a Professor with the School of Electronics and Information Engineering, BJTU. Dr. He has been a Visiting Scholar in Georgia Institute of Technology, USA, University of Southern California, USA, and Université Catholique de Louvain, Belgium. His research interests include wireless propagation channels, 5G and 6G communications. He has authored/co-authored 8 books, 5 book chapters, more than 200 journal and conference papers, as well as several patents.

Dr. He has been an Editor of the IEEE Transactions on Communications, the IEEE Transactions on Wireless Communications, the IEEE Transactions on Antennas and Propagation, the IEEE Antennas and Propagation Magazine, the IEEE Communications Letters, the IEEE Open Journal of Vehicular Technology, and a Lead Guest Editor of the IEEE Journal on Selected Area in Communications and the IEEE Transactions on Antennas and Propagation. He served as the Early Career Representative (ECR) of Commission C, International Union of Radio Science (URSI). He received the URSI Issac Koga Gold Medal in 2021, the IEEE ComSoc Asia-Pacific Outstanding Young Researcher Award in 2019, the URSI Young Scientist Award in 2015, and several Best Paper Awards in IEEE journals and conferences.

MI YANG received the M.S. and Ph.D. degrees from Beijing Jiaotong University, Beijing, China, in 2017 and 2021, respectively. He is currently an associate professor with the School of Electronics and Information Engineering, Beijing Jiaotong University. His research interests are focused on wireless channel measurement and modeling, vehicular and railway communications, and AI in channel research.

SHUN ZHOU received the Ph.D. degree in information and communication engineering from College of Electronic Science and Technology, National University of Defense Technology, Changsha, China, in 2022. He is currently an Assistant Professor with the Sixty-Third Research Institute, National University of Defense Technology. His research interests include wireless channel modeling and simulation, integrated sensing and communication channel models, and satellite-to-earth propagation channel modeling.

LONG YU received the B.S. degree in mobile communications and the M.S. degree in communications and information system from the PLA University of Science and Technology, Nanjing, China, in 2003 and 2006, respectively, and the Ph.D. degree in communications and information system from the College of Communications Engineering, Army Engineering University of PLA, Nanjing, in 2018. He is currently an Associate Research Fellow with the Sixty-Third Research Institute, National University of Defense Technology, Nanjing. His current research interests focus on wireless security, anti-jamming techniques, and game theory.

YUXIN ZHANG received the M.S. degree in communication engineering from Beijing Jiaotong University (BJTU), Beijing, China, in 2024. She is currently pursuing the Ph.D. degree with the School of Electronics and Information Engineering, BJTU, Beijing, China. Her research interests include digital twin channel and AI in wireless channel modeling.

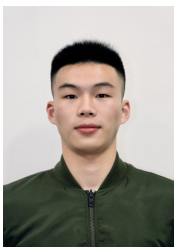

ZHICHENG QIU received the B.S. degree in communication engineering from Xiangtan University, Hunan, China, in 2022. He is currently pursuing the Ph.D. degree with the School of Electronics and Information Engineering, Beiing Jiaotong University, Beijing, China. His current research interest is artificial intelligence enabled wireless channel prediction.

ZHANGDUI ZHONG received the B.E. and M.S. degrees from Beijing Jiaotong University, Beijing, China, in 1983 and 1988, respectively. He is currently a Professor and an Advisor of Ph.D. students with Beijing Jiaotong University, where he is also the Chief Scientist of State Key Laboratory of Advanced Rail Autonomous Operation. He is the Director of the Innovative Research Team, Ministry of Education, Beijing, and the Chief Scientist of the Ministry of Railways, Beijing. He is an Executive Council Member of the Radio Association of China, Beijing, and the Deputy Director of the Radio Association, Beijing. His research interests include wireless communications for railways, control theory, and techniques for railways, and Global System for Mobile CommunicationsRailway (GSM-R) systems.

JIANHUA FAN received the Ph.D. degree from the Institute of Communication Engineering, Nanjing, China, in 1999. He is currently a Senior Researcher with the Nanjing Telecommunication Technology Research Institute, Nanjing. His research interests include wireless ad hoc networks, cognitive networks, and delay/disruption tolerant networks.